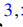# Static-to-dynamic field conversion with time-varying media

Mario Junior Mencagli [ID],[1,*] Dimitrios L. Sounas,[2,†] Mathias Fink [ID],[3,‡] and Nader Engheta [ID][4,§]

[1]*Department of Electrical and Computer Engineering, University of North Carolina, Charlotte, North Carolina 28223, USA*
[2]*Department of Electrical and Computer Engineering, Wayne State University, Detroit, Michigan 48202, USA*
[3]*Institut Langevin, ESPCI Paris, PSL University, Paris 75005, France*
[4]*Department of Electrical and Systems Engineering, University of Pennsylvania, Philadelphia, Pennsylvania 19104, USA*

We theoretically demonstrate that a uniform static electric field distribution can be partially converted to radiation fields when a portion of the medium undergoes a temporal change of its permittivity. An in-depth theoretical investigation of this phenomenon is developed for a dielectric block with a steplike temporal change located inside a waveguide charged with a DC voltage source. Closed analytical expressions are derived for the radiated electric and magnetic fields. The exchange of energy between the electrostatic and electromagnetic fields is discussed. The reconciliation between the seemingly contradictory temporal and spatial boundary conditions for the electric and magnetic fields at the interface of the time-varying dielectric block is analyzed and elucidated. Our findings may provide an alternative solution for generating electromagnetic radiation based on time-varying media.

I. INTRODUCTION

Investigations on the electrodynamics of time-varying media, which possess temporal-dependent electromagnetic parameters (permittivity and/or permeability), date back to the middle of the last century. The first investigation belongs to Morgenthaler [1], who published pioneering work on the dynamics of plane waves propagating in an unbounded homogeneous medium with a temporal-dependent refractive index. It was demonstrated that an abrupt temporal change in the medium refractive index leads to backward- and forward-propagating waves, showing the temporal analog of the spatial interface between two media with different electromagnetic parameters. Since then, other aspects of wave propagation in time-varying media, including source-dependent phenomena [2] and reflection (transmission) from (into) a semi-infinite temporal slab [3], have been explored [4]. In recent years there has been an increasing interest in time-varying media from both the engineering and the physics communities, driven primarily by the fact that they have opened the door to various interesting wave phenomena such as nonreciprocal transmission [5], virtual absorption [6,7], and temporal aiming [8], to name a few.

One particularly interesting effect in time-modulated media is conversion of static energy to radiation. In the past decades, this phenomenon, named transition scattering, was introduced by Ginzburg [9], who investigated the electromagnetic radiation generated by a stationary electron in a material modulated in time by a monochromatic acoustic wave. Subsequent works have explored a related phenomenon in plasma physics [10–14], providing an alternative method for the design of high-power sources. Demonstrating similar effects in dielectric media may open exciting opportunities for new types of sources, antennas, and energy converters.

Here, we revisit this stationary approach by treating the transient case. We demonstrate that applying an abrupt change in the electric permittivity of a dielectric slab immersed in an electrostatic field leads to controllable conversion of electrostatic energy to radiation. In contrast to previous studies [9–14], we investigate this effect through an in-depth theoretical analysis, shedding light on several aspects related to the physics of the problem such as causality and power flow. Moreover, we discuss the roles of the continuity conditions of the electric and magnetic fields' tangential components at the interface of a stationary (no time-varying) medium and a time-dependent medium, and show how they can be reconciled, overcoming a contradiction that seems to exist between them.

A conceptual representation of a time-varying dielectric structure for converting electrostatic to radiation fields is displayed in Fig. 1. Let us assume a dielectric block with permittivity ε_1 is immersed in a uniform static electric field ($\mathbf{e}_0$), as shown in Fig. 1(a). Then, we assume that the dielectric block, after it has been fully polarized by $\mathbf{e}_0$ and the system has reached the steady state, undergoes a change of its permittivity in time in a rapid-step fashion from ε_1 to ε_2, as shown in Fig. 1(b). The permittivity is assumed to be dispersionless, and both values are taken to be real positive larger than unity. The dispersionless assumption is justified assuming that the resonance frequency of the material is very high [15]. This change of the permittivity perturbs the electrostatic field distribution inside the dielectric block established by $\mathbf{e}_0$. Such perturbation results from the condition of temporal continuity

*mmencagl@uncc.edu
†dsounas@wayne.edu
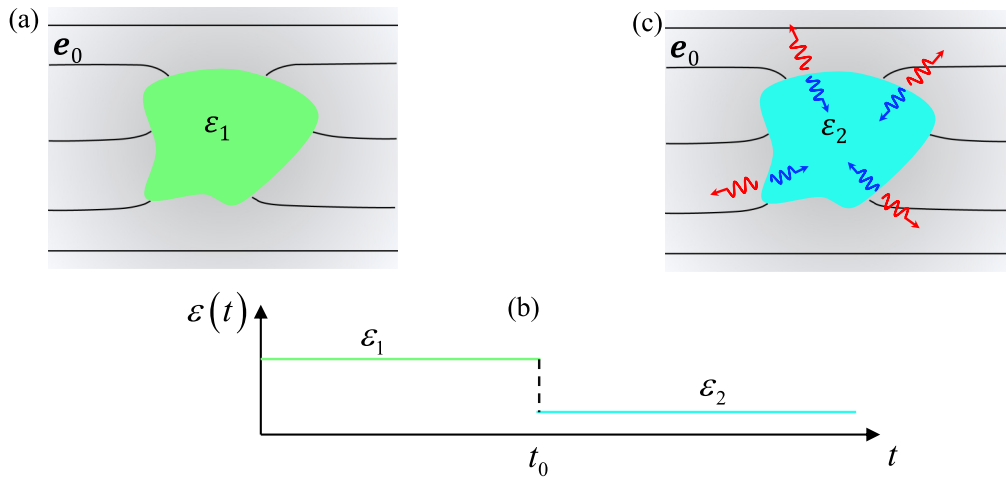‡mathias.fink@espci.fr
§engheta@seas.upenn.edu

FIG. 1. Conceptual representation of static-to-radiative field conversion based on time-varying media. (a) A time-varying dielectric block embedded in a uniform static electrostatic field $\mathbf{e}_0$. (b) Temporal profile of permittivity, which changes from a positive value ε_1 to another positive value ε_2 at $t = t_0$. (c) Sketch of the wave phenomenon generated by the change of the permittivity of the dielectric block.

of the electric displacement **d** [16] at the time instant ($t = t_0$) of changing the permittivity value. The material parameters of the region outside the dielectric are assumed to be temporally stationary, and thus no temporal boundary conditions are applied there. It might appear that the tangential components of the electrostatic field are discontinuous across the spatial boundary of the dielectric block in Fig. 1(a) when the permittivity experiences a temporal change. However, in the analysis that follows, we prove that this is not the case and the condition of spatial continuity of the tangential electric field components across the spatial boundary of a dielectric block undergoing a stepwise temporal change of permittivity is indeed satisfied through the generation of electromagnetic pulses on the boundary, which propagate on either side of the boundary and lead to partial conversion of the electrostatic field to radiation fields, as shown schematically in Fig. 1(a).

II. TIME-VARYING DIELECTRIC BLOCK IN A PARALLEL-PLATE METALLIC WAVEGUIDE CHARGED WITH A DC VOLTAGE SOURCE

We now study analytically the time-dependent feature introduced above. Without loss of generality and for the sake of simplicity, instead of considering a time-varying dielectric block standing in an open space as in Fig. 1, we focus on the parallel waveguide scenario in Fig. 2(a). The structure is assumed to be invariant along the y direction, infinite in the z direction, and bounded in the x direction. The structure consists of a time-varying dielectric rectangular block of size $2L \times d$ sandwiched between two horizontal, impenetrable [e.g., perfectly electric conducting (PEC)] walls. The regions outside the time-varying dielectric block are filled with air. In order to create a static electric field distribution inside this structure, we can imagine connecting the metallic plates to a constant (DC) voltage source (i.e., battery). After the initial transient has passed, the voltage source establishes an x-directed uniform static electric field inside the structure given by $e_x^s = V/d$, with V and d the voltage across the PEC plates and the separation between them, respectively. Once e_x^s

has been established inside the whole structure and the system has reached a steady state, the permittivity of the dielectric block is made to vary in time rapidly. We assume that the relative permittivity (ε_r) rapidly switches from one value ε_{r1} to a different one ε_{r2} (both positive values greater than unity) at $t = 0$, as shown in the inset of Fig. 2(a).

Due to the symmetry of the structure in Fig. 2(a) with respect to the plane $z = 0$ and the distribution of e_x^s, we can analyze the response of the system by solving the reduced structure in Fig. 2(b). It consists of half of the structure to the right of the symmetry plane ($z = 0$) and a perfectly magnetic conducting (PMC) wall on that plane. The field distribution on the left side of the symmetry plane will be the mirror image of that on the right side. A suitable way of solving the problem under study is to formulate it as an initial value problem of Maxwell equations for transverse electromagnetic (TEM) waves propagating in the z direction. As initial values we consider the value of the electric field at $t = 0^+$, i.e., just after the change of the permittivity, in the air and dielectric regions, given by $e_x^{sa}(z, 0^+) = e_x^s$ and $e_x^{sd}(z, 0^+) = \frac{\varepsilon_{r1}}{\varepsilon_{r2}} e_x^s$, respectively.
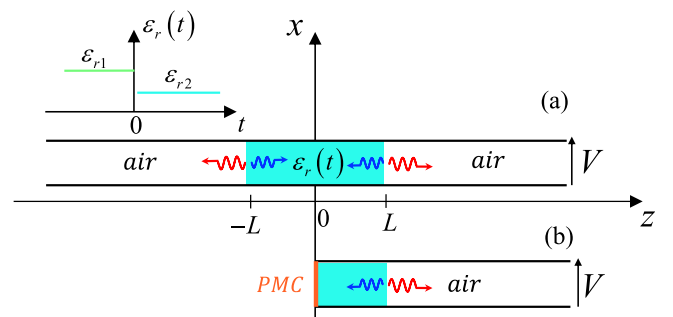
FIG. 2. Parallel waveguide scenario under study. (a) A time-varying dielectric rectangular block of size $2L \times d$ is placed at the center of a waveguide filled with air. The PEC walls of the waveguide are connected to a DC voltage source establishing uniform static electric field inside the waveguiding structure. The time-dependent relative permittivity [$\varepsilon_r(t)$] of the dielectric is shown in the inset. (b) The waveguide is terminated with a PMC wall.

FIG. 3. Spatial distribution of the electric field (a)–(d), and the Poynting vector (e)–(h), at time instants $t = 0.1T$, $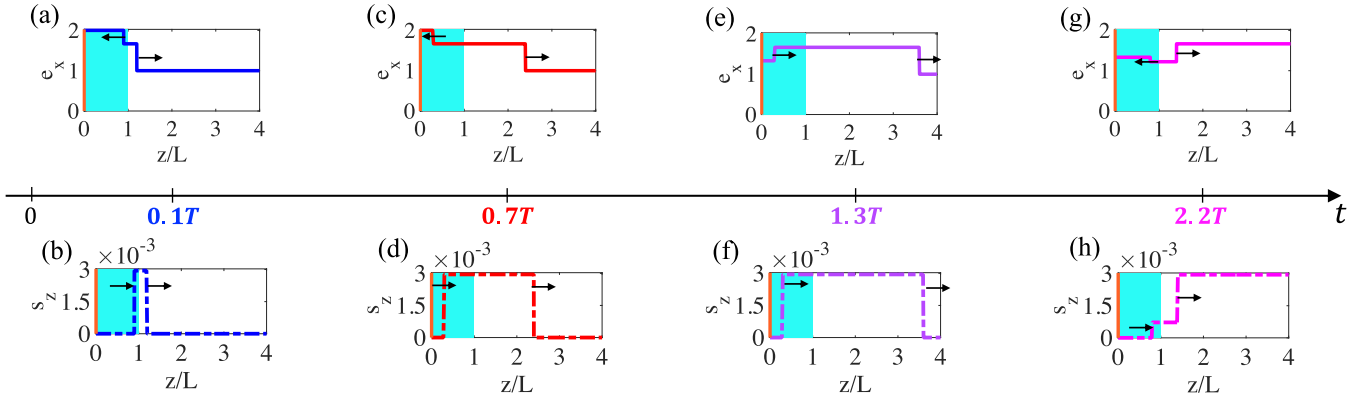0.7T$, $1.3T$, and $2.2T$ inside the waveguide of Fig. 2(b). The arrows in the top panels (a)–(d) and in the bottom panels (e)–(h) indicate the direction of propagation of the plane waves presenting into the waveguide at the considered time instants and of the corresponding Poynting vectors, respectively.

These fields are obtained by considering that across the instant $t = 0$, e_x^{sa} remains continuous while e_x^{sd} is discontinuous, modeling the disturbance caused by the permittivity change, and its value at $t = 0^+$ is obtained by imposing the temporal continuity of **d**. Solution of Maxwell equations with these initial conditions can be achieved through the Laplace transform (a complete derivation of the fields is given in Appendixes A, B, and C), leading to the following expressions for the time-dependent electric fields in the dielectric and air regions for $t > 0$:

$$e_x^a(z,t) = \frac{e_x^s \sqrt{\varepsilon_{r2}}}{1 - \sqrt{\varepsilon_{r2}}} \left(\frac{\varepsilon_{r1}}{\varepsilon_{r2}} - 1 \right) \left\{ -\gamma u\left[t - \frac{1}{c_a}(z - L) \right] + (1 - \gamma) \sum_{n=1}^{\infty} \gamma^n u\left[t - \frac{1}{c_a}(z - L) + 2nT \right] \right\} + u(t) e_x^s, \quad z \geqslant L, \quad (1)$$

$$e_x^d(z,t) = \frac{e_x^s}{\sqrt{\varepsilon_{r2}} + 1} \left(1 - \frac{\varepsilon_{r1}}{\varepsilon_{r2}} \right) \sum_{n=0}^{\infty} \gamma^n \left\{ u\left[t - \frac{1}{c_d}(L - z) - 2nT \right] + u\left[t - \frac{1}{c_d}(z + L) + 2nT \right] \right\} + u(t) \frac{\varepsilon_{r1}}{\varepsilon_{r2}} e_x^s, \quad 0 \leqslant z < L, \quad (2)$$

with c_a the speed of light in air, $c_d = c_a/\sqrt{\varepsilon_{r2}}$, $\gamma = (\sqrt{\varepsilon_{r2}} - 1)/(\sqrt{\varepsilon_{r2}} + 1)$ (reflection coefficient at section $z = L$ assuming the incident wave coming from the dielectric region), $u(\alpha)$ is the Heaviside unit function, which equals 1 for $\alpha > 0$ and zero for $\alpha < 0$, and $T = L/c_d$ is the time of propagation between the air-dielectric interface and the magnetic wall. Equations (1) and (2) can be viewed as a superposition of static and dynamic electric fields. The term $u(t)$ represents the static electric field with amplitude equal to the corresponding region's initial value. The dynamic electric field consists of an infinite number of waves traveling along the z axis with different amplitudes and a time delay $2T$ from each other, equal to the time it takes a wave to propagate through the dielectric slab. As expected, Eq. (1), describing the air region's electric field, contains plane waves of the form $u[t - \frac{1}{c_{air}}(z - L) + 2nT]$, which propagate outward from the air-dielectric interface ($z = L$). On the other hand, Eq. (2), describing the dielectric region's electric field, contains an infinite number of plane waves of the form $u[t - \frac{1}{c_d}(L \pm z) \pm 2nT]$, which propagate both inward and outward from the same interface, as a result of reflection on the two boundaries of the dielectric slab (the air-dielectric interface and the PMC wall). Using Eqs. (1) and (2), and the time-dependent Maxwell equations, it is straightforward to also calculate the magnetic field in the dielectric and air regions. As shown in Appendix B, in both regions, the magnetic

field, as expected, is directed along the y axis and is dynamic only [its expression does not contain terms with $u(t)$]. The analytical expressions for both the electric and magnetic fields have been validated through comparison against numerical solutions (Appendix B).

To get a better understanding of the temporal evolution of this wave phenomenon and the associated energy flow, we now look into the spatial distribution of the electric field and the instantaneous Poynting vector inside the waveguide at four different time instants ($t = 0.1T$, $0.7T$, $1.3T$, $2.2T$). Hereafter, we assume that the length of the dielectric block is L and its relative permittivity changes from $\varepsilon_{r1} = 8$ to $\varepsilon_{r2} = 4$. The spacing and the DC voltage between the waveguide metallic plates are $d = 1$ mm and $V = 1$ V, respectively. With this spacing and voltage, at the steady state the electrostatic field inside the waveguide is uniform and equal to 1 V/mm. As mentioned earlier, the change of the dielectric-block permittivity occurs at $t = 0$. According to the temporal boundary conditions, this change perturbs the electrostatic field distribution in the dielectric region, transforming its value from 1 to 2 V/mm, while the value of the electrostatic field in the air region is still equal to 1 V/mm. Now, observing the spatial distribution of the electric field a bit after $t = 0$, say $t = t_1 = 0.1T$, shown in Fig. 3(a), we notice that there is a region across the air-dielectric interface where the electric field is between 1 and 2 V/mm. Quite importantly, the electric

field is continuous across the spatial boundary, as required by the spatial boundary conditions. From Eqs. (1) and (2), we can identify this field with the plane waves $2/3u[t_1 - (z-L)/c_a]$ and $-1/3u[t_1 - (L-z)/c_d]$, propagating in opposite directions off the dielectric-air interface with velocities equal to the wave velocities in the two media. Figure 3(e) displays the z component of the instantaneous Poynting vector (S_z) at the same time instance ($t = t_1$) as Fig. 3(a). The other components of the Poynting vector are equal to zero as we are considering TEM plane waves with respect to the z axis. By comparing Figs. 3(a) and 3(e), one can observe that, as expected, S_z is different than zero only in the region between the two wavefronts and points in the positive z direction, showing power flow from the dielectric medium to air. Hence, the right-going plane wave, propagating in the air region along the positive z axis, is a standard forward wave. On the other hand, the left-going plane wave, propagating in the dielectric region along the negative z axis, is a backward wave. At $t = t_2 = 0.7T > t_1$, the two plane waves ($2/3u[t_2 - (z-L)/c_a]$ and $-1/3u[t_2 - (L-z)/c_d]$) have propagated even further from the air-dielectric interface as highlighted by the position of their wavefronts [see Fig. 3(b)], and a greater presence of electromagnetic energy movement is observed in the waveguide [see Fig. 3(f)]. At $t = T$ (T the time delay introduced by the dielectric block), the plane wave, $-1/3u[T - (L-z)/c_d]$, propagating inside the dielectric, hits the perfect magnetic wall located at $z = 0$, generating a second plane wave, represented by $-1/3u[t - (z+L)/c_d]$ in Eq. (2), which is added to the electric field established by the first wave $-1/3u[t_2 - (L-z)/c_d]$, resulting in a field distribution as in Fig. 3(c). On the other hand, in the air region there is still the same plane wave ($2/3u[t_3 - (z-L)/c_a]$) that was propagating in it during the previous time interval ($0 < t < T$), which is perturbing the electrostatic field distribution established by the voltage source. From Fig. 3(g), which displays the distribution of S_z into the waveguide at the same time instant ($t = t_3$) of the electric field in Fig. 3(c), we notice that S_z is positive also at this time instant, showing flow of energy from the dielectric to air. At $t = 2T$, the plane wave $-1/3u[t - (z+L)/c_d]$ propagating in the dielectric reaches the air-dielectric interface (section $z = L$) and experiences a reflection, resulting in a pulse again propagating toward the PMC wall in the dielectric region ($-1/9u[t - (L-z)/c_d - 2T]$) and another pulse that perturbs the field in the air region ($-4/9u[t - (z-L)/c_a + 2T]$), as can be seen in Fig. 3(d). At the same time, the direction of power flow is still from the dielectric to air region [see Fig. 3(h)]. As time passes, due to the spatial boundaries located at $z = 0$ (perfect magnetic wall) and $z = L$ (air-dielectric interface), the number of plane waves propagating into the waveguide increases as described by the summations in Eqs. (1) and (2). However, all waves in both regions always carry power from the dielectric to air region. At $t \to \infty$, the amplitudes of the plane waves, given by $|\gamma|^n$, decay to zero, since $|\gamma| < 1$, and the electric field converges to the uniform static electric field (e_x^s) established inside the waveguide by the DC voltage source. This point highlights the transitory nature of the wave phenomenon induced by the change of the dielectric-block permittivity, which generates a series of plane waves whose amplitude

vanishes after some time and the system returns to its steady state (see Appendix C). The Fourier transform of the electric field in the air region [Eq. (1)] assumes the shape of a sinclike function, and is derived and discussed in Appendix G.

III. ENERGY EXCHANGE BETWEEN THE TIME-VARYING DIELECTRIC BLOCK AND THE RADIATED WAVES

We now turn to the discussion of energy exchange happening in the system as a consequence of the permittivity change of the dielectric block. To this end, we consider $W = |\mathbf{d}|^2 L/(2\varepsilon)[\mathrm{J/m^2}]$, which is the electric energy density stored in an electrostatic field distribution in a dispersionless dielectric medium with permittivity ε and length L. By means of the previous equation, it is straightforward to derive the electric energy densities associated to the electrostatic field in the dielectric block before ($t = 0^-$) and after ($t = 0^+$) the permittivity change. These energy densities are $W_{0^-} = \frac{1}{2}\varepsilon_0\varepsilon_{r1}L(\frac{V}{d})^2$ and $W_{0^+} = \frac{1}{2}\varepsilon_0\frac{\varepsilon_{r1}^2}{\varepsilon_{r2}}L(\frac{V}{d})^2$ at $t = 0^-$ and $t = 0^+$, respectively, with the latter derived from the continuity of $\mathbf{d}$ across the temporal boundary at $t = 0$. Taking the difference between W_{0^+} and W_{0^-}, we find $\Delta W_0 = \frac{1}{2}\varepsilon_0\varepsilon_{r1}L(\frac{\varepsilon_{r1}}{\varepsilon_{r2}} - 1)(\frac{V}{d})^2$, which gives the energy supplied to or taken from the system upon the change of the permittivity by an external agent performing this change. For $\varepsilon_{r1} > \varepsilon_{r2}$, which is the case discussed so far with $\varepsilon_{r1} = 8$ and $\varepsilon_{r2} = 4$, $\Delta W_0 > 0$ implying that the permittivity change increases the electric energy density inside the dielectric block. This means that the external agent provides energy to the dielectric block when changing its permittivity. The second mechanism of energy exchange occurs between the electrostatic energy in the dielectric block and the electromagnetic energy propagating in the system. The energy balance of this mechanism can be expressed as the difference between the electric energy density in the dielectric block at $t = 0^+$ and after the transient time, that is, at $t \to \infty$. As discussed earlier, at $t \to \infty$ the system has returned to a steady state with a uniform static field distribution (V/d) and, as a result, the electric energy density in the dielectric block is given by $W_\infty = \frac{1}{2}\varepsilon_0\varepsilon_{r2}L(\frac{V}{d})^2$. Therefore, the energy balance is $\Delta W_\infty = \frac{1}{2}\frac{\varepsilon_0}{\varepsilon_{r2}}L(\varepsilon_{r2}^2 - \varepsilon_{r1}^2)(\frac{V}{d})^2$. For $\varepsilon_{r1} > \varepsilon_{r2}$, $\Delta W_\infty < 0$ meaning that the dielectric block loses part of its energy, which is released in the form of electromagnetic energy traveling away from the dielectric block. Indeed, as discussed above and shown in Figs. 3(e)–3(h), the plane waves, produced by the permittivity change, propagating in the waveguide have a Poynting vector along the positive z axis and, therefore, carry energy from the dielectric to the air region. The total radiated energy density, given by the infinite set of plane waves, is equal to $-\Delta W_\infty$ (Appendix F), highlighting that the difference between the electrostatic energy in the dielectric block at $t = 0^+$ and $t \to \infty$ is fully released in the form of electromagnetic energy in the air region.

So far, the discussion has focused on the case $\varepsilon_{r1} > \varepsilon_{r2}$. As for the case with $\varepsilon_{r1} < \varepsilon_{r2}$, quite interestingly, the energy flows in the opposite direction: from the air region to the dielectric region. The plane waves traveling in the air region carry energy to the dielectric block until the system reaches
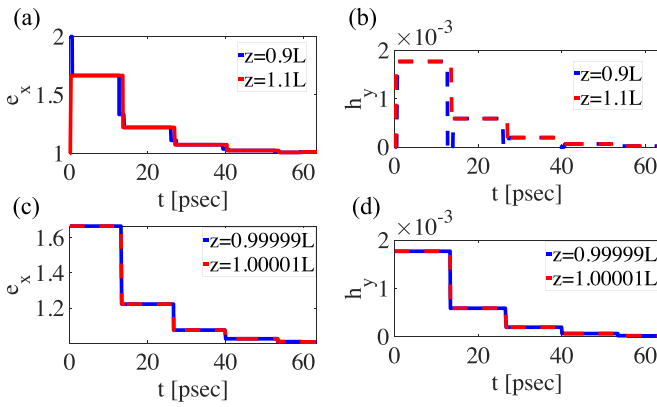
FIG. 4. Temporal evolution of the electric field, (a), (c), and the magnetic field, (b), (d), at the observation points $z = 0.9L$, $z = 1.1L$ and $z = 0.999\,99L$, $z = 1.0001L$, respectively.

the steady state, which is the same as the initial state. A complete and detailed discussion of the case $\varepsilon_{r1} < \varepsilon_{r2}$ is provided in Appendix E.

IV. SPATIAL BOUNDARY CONDITIONS AT THE INTERFACE OF A TIME-VARYING DIELECTRIC BLOCK EMBEDDED IN A UNIFORM STATIC ELECTRIC FIELD

In the last part of this work, we will focus on the spatial-continuity condition of the tangential components of electric and magnetic fields across the air-dielectric interface in the waveguide in Fig. 2(a) after the change of the permittivity of the dielectric block ($t > 0$) from $\varepsilon_{r1} = 8$ to $\varepsilon_{r2} = 4$. To this end, we plot e_x [from Eqs. (1) and (2)] and h_y [from Eqs. (B17) and (B18) in Appendix B] as a function of time at different observation points before and after the section $z = L$. Figures 4(a) and 4(b) show the temporal evolution of e_x and h_y, respectively, evaluated at the locations $z = 0.9L$ and $z = 1.1L$. As discussed before, the amplitude of e_x decays as time passes and after the transient time its value returns to 1. Analogous behavior is observed for h_y [Fig. 4(b)]; its amplitude converges to zero after the transient time. As can be seen from Fig. 4(a) [Fig. 4(b)], the temporal profiles of e_x (h_y) evaluated at $z = 0.9L$ and $z = 1.1L$ do not overlap with each other. Therefore, e_x and h_y seem to be discontinuous across the air-dielectric interface ($z = L$). However, moving the observation points even closer to $z = L$, such as $z = 0.999\,99L$ and $z = 1.000\,01L$, the temporal profiles of e_x (h_y) at these two locations overlap with each other as shown in Fig. 4(c) [Fig. 4(d)]. More rigorously, it can be mathematically shown (Appendix D) that for time instants very close to $t = 0$, yet with finite values, there is always a region around the air-dielectric interface within which the fields are continuous, as they should be. These results show that that the condition of the spatial continuity of the tangential components of the fields across a time-varying dielectric block embedded in a uniform static electric field is satisfied as expected.

We emphasize that the phenomenon of static-to-dynamic field conversion with time-varying media described in this manuscript essentially remains even for slow permittivity

changes if the permittivity transition time is much smaller than T. Additional results in this regard and a discussion on potential pathways for experimental verifications are provided in Appendixes H and I.

V. CONCLUSIONS

In conclusion, we have shown, using an analytical approach, how the static-to-dynamic field conversion can be achieved through a time-varying dielectric block embedded in an electrostatic field distribution. Such dielectric block experiencing a change of its permittivity in time gives rise to radiation fields. These fields start propagating into the system from the spatial boundary of the time-varying material enforced by the continuity of the electric and magnetic fields' tangential components at such boundary. The radiation fields carry the energy away from (into) the time-varying dielectric block when decreasing (increasing) its permittivity. The results presented here might find applications in the design of electromagnetic sources in integrated systems, similar to sources that have been demonstrated in the past in plasmas.

APPENDIX A: INITIAL VALUE PROBLEM FOR PLANE WAVES

This Appendix shows an analytical solution to the Maxwell equations for TEM waves constrained by an initial value defining the electric field's value at the initial time instant, say, $t = 0^+$. Let $e_x(t, z)$ and $h_y(t, z)$ be the electric and magnetic fields of a z-propagating TEM wave. For $t < 0$, the electric field is equal to the DC field and the magnetic field is zero. The fields satisfy the Maxwell equations,

$$\frac{\partial e_x(t, z)}{\partial z} + \mu \frac{\partial h_y(t, z)}{\partial t} = 0, \qquad (A1)$$

$$\frac{\partial h_y(t, z)}{\partial z} + \varepsilon \frac{\partial e_x(t, z)}{\partial t} = 0, \qquad (A2)$$

with ϵ and μ the permittivity and the permeability of the medium, respectively. The aim now is to solve these coupled differential equations for $t > 0$ by taking into account the electric field's initial value at $t = 0^+$. A suitable way to solve this problem is with the use of the Laplace transform of $e_x(t, z)$ and $h_y(t, z)$ with respect to t: $E_x(s, z) = \int_0^\infty e_x(t, z)e^{-st}dt$, $H_y(s, z) = \int_0^\infty h_y(t, z)e^{-st}dt$. Applying these transformations to Eqs. (A1) and (A2), and using the differentiation properties of the Laplace transform [17] we get

$$\frac{\partial E_x(s, z)}{\partial z} + s\mu H_y(s, z) = 0, \qquad (A3)$$

$$\frac{\partial H_y(s, z)}{\partial z} + \varepsilon s E_x(s, z) - \varepsilon e_x(0^+, z) = 0, \qquad (A4)$$

with $e_x(0^+, z)$ the electric field's value at $t = 0^+$. Eliminating $H_y(s, z)$ from the previous equations, an ordinary, inhomogeneous, differential equation for $E_x(s, z)$ is obtained, in which s is treated as a parameter,

$$\frac{\partial^2 E_x(z, s)}{\partial z^2} - k^2 E_x(z, s) = \xi(z, s), \tag{A5}$$

with $k = s/c$, $c = 1/\sqrt{\epsilon \mu}$, and $\xi(s, z) = -\frac{k^2}{s} e_x(0^+, z)$. The solution of Eq. (A5) is [17]

$$E_x(s, z) = c_1 e^{kz} + c_2 e^{-kz} + \frac{e^{kz}}{2k} \int e^{-kz} \xi(z, s) dz$$
$$- \frac{e^{-kz}}{2k} \int e^{kz} \xi(z, s) dz, \tag{A6}$$

with c_1 and c_2 constants that are to be determined from the spatial boundary conditions. Equation (A6) represents the electric field of a plane wave in the Laplace domain constrained by the initial value $e_x(z, 0^+)$.

APPENDIX B: ANALYTICAL SOLUTION

Here, building on the discussion of the previous Appendix, we provide an analytical solution of the transient electric and magnetic fields resulting from the abrupt temporal change of the relative permittivity [$\varepsilon_r(t)$] of the dielectric block in the waveguiding system of Fig. 2(b). As discussed in the main text, it is assumed that $\varepsilon_r(t)$ suddenly varies between two positive values at $t = 0$, once the DC voltage source, connected to the metallic plates, has already established a uniform static electric field (e_x^s) inside the waveguide. The change of permittivity results in a jump of the electrostatic field inside the dielectric block, which can be derived by applying the continuity of **d** at $t = 0$, as $\mathbf{d}_{-\delta} = \mathbf{d}_\delta$ in the limit when $\delta \to 0$. Based on this, the electrostatic field inside the dielectric block

at $t = 0^+$ (right after the permittivity change) is found:

$$e_x^{sd} = \frac{\varepsilon_{r1}}{\varepsilon_{r2}} e_x^s. \tag{B1}$$

On the other hand, the permittivity in the air region does not change, and the electrostatic field stays continuous across $t = 0$ and its value at $t = 0^+$ reads

$$e_x^{sa} = e_x^s. \tag{B2}$$

These initial values (e_x^{sd} and e_x^{sa}), which model the disturbance caused by the permittivity change of a portion of the medium inside the waveguide, can be used in the initial value problem discussed in the previous Appendix to study the temporal evolution of the system for $t > 0$.

1. Laplace domain

Plugging the initial values of Eqs. (B1) and (B2) into Eq. (A6), we can readily derive the electric field in the dielectric and air regions in the Laplace domain,

$$E_x^d(s, z) = A e^{k_d z} + B e^{-h_d z} + \frac{1}{s} \frac{\varepsilon_{r1}}{\varepsilon_{r2}} e_x^s \quad 0 \leqslant z \leqslant L, \tag{B3}$$

$$E_x^a(s, z) = C e^{k_a z} + D e^{-k_a z} + \frac{1}{s} e_x^s \quad z \geqslant L, \tag{B4}$$

with c_a the speed of light in free space, $k_{a,d} = s/c_{a,d}$, and $c_d = c_a/\sqrt{\varepsilon_{r2}}$. The magnetic field in both regions (H_y^d and H_y^a) can be derived from Eqs. (A3) and (A4). The four unknown constants (A, B, C, D) can be obtained by applying the conservation of the transverse components of the electric and magnetic fields at the interface $z = L$ [see Fig. 2(b)], zeroing the tangential components of the magnetic field at the interface $z = 0$, and the radiation condition at $z \to \infty$. In doing so, we obtain the following expressions for the electric and magnetic fields in the two regions:

Electric field:

$$E_x^d(s, z) = e_x^s \frac{1}{s} \left(1 - \frac{\varepsilon_{r1}}{\varepsilon_{r2}}\right) \left[\frac{k_a(e^{k_d z} + e^{-k_d z})}{k_a(e^{k_d L} + e^{-k_d L}) + k_d(e^{k_d L} - e^{-k_d L})}\right] + \frac{1}{s} \frac{\varepsilon_{r1}}{\varepsilon_{r2}} e_x^s \quad 0 \leqslant z \leqslant L, \tag{B5}$$

$$E_x^a(s, z) = e_x^s \frac{e^{k_a(L-z)}}{s} \left(-1 + \frac{\varepsilon_{r1}}{\varepsilon_{r2}}\right) \left[\frac{k_d(e^{k_d L} - e^{-k_d L})}{k_a(e^{k_d L} + e^{-k_d L}) + k_d(e^{k_d L} - e^{-k_d L})}\right] + \frac{1}{s} e_x^s \quad z > L. \tag{B6}$$

Magnetic field:

$$H_y^d(s, z) = e_x^s \frac{k_a}{\mu_0 s^2} \left(-1 + \frac{\varepsilon_{r1}}{\varepsilon_{r2}}\right) \left[\frac{k_d(e^{k_d z} - e^{-k_d z})}{k_a(e^{k_d L} + e^{-k_d L}) + k_d(e^{k_d L} - e^{-k_d L})}\right] \quad 0 \leqslant z \leqslant L, \tag{B7}$$

$$H_y^a(s, z) = e_x^s \frac{e^{k_a(L-z)}}{\mu_0 s^2} \left(-1 + \frac{\varepsilon_{r1}}{\varepsilon_{r2}}\right) \left[\frac{k_a k_d(e^{k_d L} - e^{-k_d L})}{k_a(e^{k_d L} + e^{-k_d L}) + k_d(e^{k_d L} - e^{-k_d L})}\right] \quad z > L, \tag{B8}$$

with μ_0 the free space permeability. The remaining difficulty is transforming the expressions of the derived fields in the Laplace domain to the time domain, which is the subject of the next section.

2. Time domain

The most common technique for performing the inverse Laplace transform of complex functions consists of evaluating a contour integral with the residue theorem [18]. Although

such technique can be applied to Eqs. (B5)–(B8), we have followed a different way: reducing such equations into a composition of functions whose inverse Laplace transform is known. Let us begin with the electric field in the dielectric region [Eq. (B5)]. The right-hand side of Eq. (B5) exhibits a singular behavior in the complex s plane at $s = 0$ and $s_m = \frac{c_d}{2L}(\ln \gamma + 2im\pi)$ with $m = 0, \pm1, \pm2, \ldots, i = \sqrt{-1}$, and $\gamma = \frac{\sqrt{\varepsilon_{r2}} - 1}{\sqrt{\varepsilon_{r2}} + 1}$ (the reflection coefficient at the air-dielectric interface). It is straightforward to show that these singular-

ities are poles of E_x^d and, as $0 \leqslant |\gamma| < 1$, they lie in the open left half of the complex s plane including the imaginary axis. Therefore, expressing $s = \sigma + i\omega$ (σ and ω are two real numbers), the existence region of E_x^d, which defines the set of s values where the integral in the definition of Laplace transform converges [18], is given by $\sigma > 0$. Since this region does not include the imaginary axis of the s plane ($\sigma = 0$), one can state that the inverse Laplace transform of E_x^d, corresponding to the time-domain electric field [$e_x^d(t, z)$], is only marginally stable. Nevertheless, $e_x^d(t, z)$ asymptotically (for $t \to \infty$) converges to a finite value, as will be shown later.

After discussing the existence region and the stability of E_x^d, we proceed to carry out its inverse Laplace transform. Substituting $k_{a,d} = s/c_{a,d}$ in Eq. (B5) and simplifying, we obtain

$$E_x^d(s, z) = \frac{e_x^s}{s}\left(1 - \frac{\varepsilon_{r1}}{\varepsilon_{r2}}\right)\left(e^{\frac{s}{c_d}(z-L)} + e^{-\frac{s}{c_d}(z+L)}\right)$$

$$\times \frac{e^{2\frac{s}{c_d}L}}{e^{2\frac{s}{c_d}L}(\sqrt{\varepsilon_{r2}} + 1) + 1 - \sqrt{\varepsilon_{r2}}} + \frac{1}{s}\frac{\varepsilon_{r1}}{\varepsilon_{r2}}e_x^s. \quad \text{(B9)}$$

By inspecting the previous equation, with

$$Q \equiv \frac{e^{2\frac{s}{c_d}L}}{e^{2\frac{s}{c_d}L}(\sqrt{\varepsilon_{r2}} + 1) + 1 - \sqrt{\varepsilon_{r2}}}, \quad \text{(B10)}$$

one can notice that except for Q the other terms are in the form for which the inverse Laplace transform is known. Replacing

$e^{2\frac{s}{c_d}L}$ with $1/w$ in Eq. (B10) and rearranging, we get

$$Q = \frac{1}{1 + \sqrt{\varepsilon_{r2}}}\frac{1}{1 - \gamma w}. \quad \text{(B11)}$$

The second term in the previous equation can be expanded as a geometric series with an argument $(-\gamma w)$. Therefore, Q can be rewritten as

$$Q = \frac{1}{1 + \sqrt{\varepsilon_{r2}}}(1 + \gamma w + \gamma^2 w^2 + \gamma^3 w^3 + \cdots)$$

$$= \frac{1}{1 + \sqrt{\varepsilon_{r2}}}\sum_{n=0}^{\infty}(\gamma w)^n. \quad \text{(B12)}$$

As is well known, the geometric series converges when the absolute value of its argument is smaller than 1. This condition for the series in Eq. (B12) implies $|\gamma w| < 1$. Substituting $w = e^{-2\frac{s}{c_d}L}$, $s = \sigma + i\omega$, and $\gamma = \frac{\sqrt{\varepsilon_{r2}}-1}{\sqrt{\varepsilon_{r2}}+1}$ in the previous inequality and solving for σ, we obtain

$$\sigma > -\frac{c_d}{2L}\ln\left(\frac{\sqrt{\varepsilon_{r2}} + 1}{\sqrt{\varepsilon_{r2}} - 1}\right), \quad \text{(B13)}$$

which defines the region of convergence in the s plane for the series in Eq. (B12). For $\varepsilon_{r2} \geqslant 1$, which is the case considered in this work, the right-hand side of the previous inequality will always be a negative real number. As a result, the inequality in (B13) holds for any complex value inside the existence region of E_x^d, which, as discussed above, is given by $\sigma > 0$, and Q in Eq. (B9) can be expressed as in Eq. (B12) to perform the inverse Laplace transform of E_x^d [Eq. (B9)]. Substituting Eq. (B12) in Eq. (B9) and rearranging, we obtain

$$E_x^d(s, z) = \frac{e_x^s}{\sqrt{\varepsilon_{r2}} + 1}\left(1 - \frac{\varepsilon_{r1}}{\varepsilon_{r2}}\right)\frac{1}{s}\left[\sum_{n=0}^{\infty}\gamma^n\left(e^{\frac{s}{c_d}[z-(2n+1)L]} + e^{-\frac{s}{c_d}[z+(2n+1)L]}\right)\right] + \frac{1}{s}\frac{\varepsilon_{r1}}{\varepsilon_{r2}}e_x^s. \quad \text{(B14)}$$

Now, the time-domain expression of E_x^d can be easily carried out through the standard Laplace transform table. In doing so, we obtain

$$e_x^d(t, z) = \frac{e_x^s}{\sqrt{\varepsilon_{r2}} + 1}\left(1 - \frac{\varepsilon_{r1}}{\varepsilon_{r2}}\right)\sum_{n=0}^{\infty}\gamma^n\left\{u\left[t - \frac{1}{c_d}(L - z) - 2nT\right] + u\left[t - \frac{1}{c_d}(z + L) - 2nT\right]\right\} + u(t)\frac{\varepsilon_{r1}}{\varepsilon_{r2}}e_x^s \quad 0 \leqslant z < L. \quad \text{(B15)}$$

Following the procedure discussed to derive $e_x^d(z, t)$, we have carried out the inverse Laplace transform of the electric field in the air region [Eq. (B6)], and its time-domain expression reads

$$e_x^a(t, z) = \frac{e_x^s\sqrt{\varepsilon_{r2}}}{1 - \sqrt{\varepsilon_{r2}}}\left(\frac{\varepsilon_{r1}}{\varepsilon_{r2}} - 1\right)\left\{-\gamma u\left[t - \frac{1}{c_a}(z - L)\right] + (1 - \gamma)\sum_{n=1}^{\infty}\gamma^n u\left[t - \frac{1}{c_a}(z - L) - 2nT\right]\right\} + u(t)e_x^s \quad z \geqslant L. \quad \text{(B16)}$$

Regarding the inverse Laplace transform of the magnetic field in the air and dielectric regions [Eqs. (B7) and (B8)], the procedure adopted for the electric field can be followed. However, as we have already derived the time-domain electric field in both regions, it is more convenient to go through the time-dependent Maxwell equations. Using Eqs. (B15) and (B16) with the Maxwell equation (A1), one can derive the time-dependent magnetic field in both regions,

$$h_y^d(t, z) = \frac{1}{\mu_0 c_d}\frac{e_x^s}{\sqrt{\varepsilon_{r2}} + 1}\left(1 - \frac{\varepsilon_{r1}}{\varepsilon_{r2}}\right)\sum_{n=0}^{\infty}\gamma^n\left[-u\left(t - \frac{L - z}{c_d} - 2nT\right) + u\left(t - \frac{z + L}{c_d} - 2nT\right)\right] \quad 0 \leqslant z < L, \quad \text{(B17)}$$

$$h_y^a(t, z) = \frac{e_x^s}{\mu_0 c_a}\frac{\sqrt{\varepsilon_{r2}}}{1 - \sqrt{\varepsilon_{r2}}}\left(\frac{\varepsilon_{r1}}{\varepsilon_{r2}} - 1\right)\left[-\gamma u\left(t - \frac{z - L}{c_a}\right) + (1 - \gamma)\sum_{n=1}^{\infty}\gamma^n u\left(t - \frac{z - L}{c_a} - 2nT\right)\right] \quad z \geqslant L, \quad \text{(B18)}$$

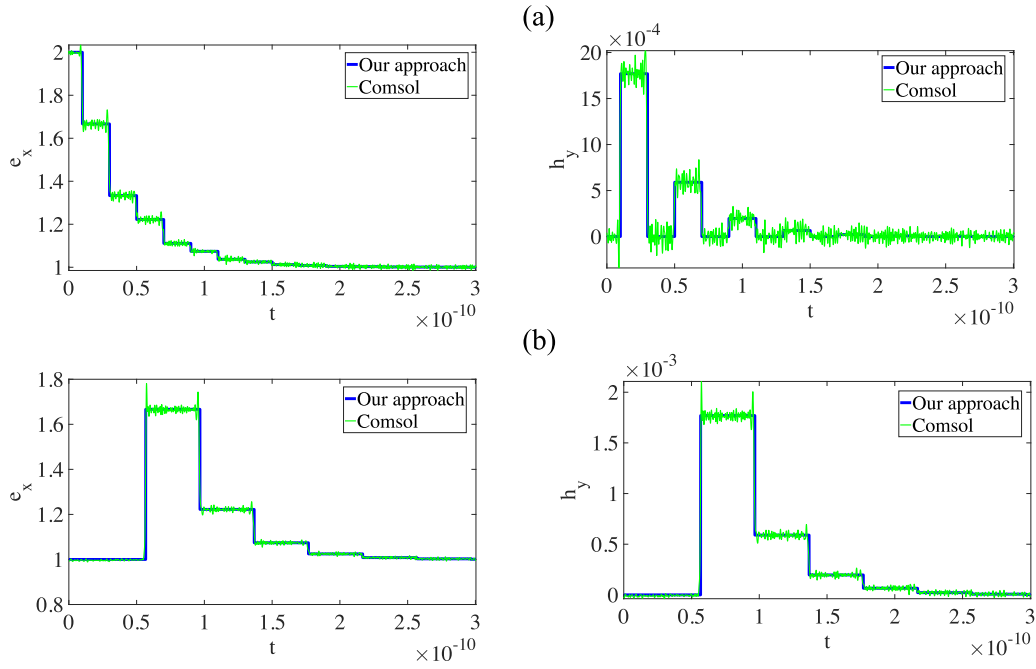with μ_0 the free space permittivity.

FIG. 5. Analytical and numerical distribution of the electric and magnetic fields at the location $z = 1.5$ mm (a) and $z = 20$ mm (b).

It is important to note that when the dielectric block is changed to free space ($\varepsilon_{r2} = 1$), the spatial boundary at the section $z = L$ disappears, and as a result, the reflection coefficient (γ) at the same section becomes zero. With this setup, Eqs. (B15)–(B18) reduce to

$$e_x^d(t, z) = \frac{e_x^s}{2}(1 - \varepsilon_{r1})\left[u\left(t - \frac{L - z}{c_a}\right) + u\left(t - \frac{z + L}{c_a}\right)\right] + \varepsilon_{r1}e_x^s u(t) \quad 0 \leqslant z < L, \tag{B19}$$

$$e_x^a(t, z) = \frac{e_x^s}{2}(\varepsilon_{r1} - 1)\left[u\left(t - \frac{z - L}{c_a}\right) - u\left(t - \frac{z + L}{c_a}\right)\right] + e_x^s u(t) \quad z \geqslant L, \tag{B20}$$

$$h_y^d(t, z) = \frac{e_x^s}{2\mu_0 c_a}(1 - \varepsilon_{r1})\left[-u\left(t - \frac{L - z}{c_a}\right) + u\left(t - \frac{z + L}{c_a}\right)\right] \quad 0 \leqslant z < L, \tag{B21}$$

$$h_y^a(t, z) = \frac{e_x^s}{2\mu_0 c_a}(\varepsilon_{r1} - 1)\left[u\left(t - \frac{z - L}{c_a}\right) - u\left(t - \frac{z + L}{c_a}\right)\right] \quad z \geqslant L, \tag{B22}$$

respectively. Comparing Eqs. (B15)–(B18) with Eqs. (B19)–(B22), one can observe that, as expected, the multiple reflection process, undergoing for $\varepsilon_{r2} > 1$ (see discussion in the main text), does not happen for $\varepsilon_{r2} = 1$. For $0 < t < L/c_a$, the dynamic electric field into the waveguiding system can be identified with the plane waves, $\frac{e_x^s}{2}(1 - \varepsilon_{r1})u(t - \frac{L-z}{c_a})$ and $\frac{e_x^s}{2}(\varepsilon_{r1} - 1)u(t - \frac{z-L}{c_a})$ [see Eqs. (B19) and (B20)], propagating in opposite directions off $z = L$. The former wave, hitting the PMC wall at $t = L/c_a$, gives rise to another wave, $\frac{e_x^s}{2}(\varepsilon_{r1} - 1)u(t - \frac{z+L}{c_a})$ [see Eq. (B19)], propagating in the same region ($0 \leqslant z \leqslant L$) but in the opposite direction (along the positive z axis). This wave reaches the boundary $z = L$ at $t = 2L/c_a$, and as $\gamma = 0$, in contrast to the case with $\varepsilon_{r2} > 1$, it does not experience any reflections (no reflected waves) and results in the wave $\frac{e_x^s}{2}(\varepsilon_{r1} - 1)u(t - \frac{z+L}{c_a})$ [see Eq. (B20)] propagating in the region $z \geqslant L$ for $t > 2L/c_a$.

3. Analytical vs numerical solutions

A numerical simulation of the waveguiding system in Fig. 2(b) has been carried out using the time-domain solver of the commercial software COMSOL MULTIPHYSICS. A lumped port, connected on the opposite side of the PMC wall, has been used to establish an electrostatic field equal to $e_x^s = 1$ V/mm between the PEC walls at a distance $d = 1$ mm apart. The relative permittivity of the dielectric block, which is $L = 3$ mm long, changes abruptly from $\varepsilon_{r1} = 8$ to $\varepsilon_{r2} = 4$. This sudden change has been modeled through a steplike function with two continuous derivatives to ensure the convergence of the simulation. Figures 5(a) and 5(b) compare the analytical and numerical distribution of the electric and magnetic fields as a function of time at locations $z = 1.5$ mm and $z = 20$ mm, respectively. The numerical solutions (continuous green lines) agree well with the analytical solutions (continuous blue lines) obtained from Eqs. (B15)–(B18). The numerical solutions

are slightly oscillating compared to the analytical solutions. This small difference between the two solutions can be attributed to the intrinsic low-pass response of the numerical solutions.

APPENDIX C: THE LIMIT $t \to \infty$

In this section, we discuss the time evolution of the fields for $t \to \infty$. Recalling that $\lim_{t \to \infty} u(t - a) = 1$ with $a \in \mathbb{R}$, Eqs. (B15) and (B16) for $t \to \infty$ reduce to

$$
\begin{aligned}
e_x^d(t \to \infty, z) = {} & \frac{2e_x^s}{\sqrt{\varepsilon_{r2}} + 1}\left(1 - \frac{\varepsilon_{r1}}{\varepsilon_{r2}}\right)\sum_{n=0}^{\infty} \gamma^n \\
& + \frac{\varepsilon_{r1}}{\varepsilon_{r2}}e_x^s \quad 0 \leqslant z < L,
\end{aligned} \tag{C1}
$$

$$
\begin{aligned}
e_x^a(t \to \infty, z) = {} & e_x^s \frac{\sqrt{\varepsilon_{r2}}}{1 - \sqrt{\varepsilon_{r2}}}\left(\frac{\varepsilon_{r1}}{\varepsilon_{r2}} - 1\right) \\
& \times \left[-\gamma + (1 - \gamma)\sum_{n=0}^{\infty} \gamma^n - (1 - \gamma)\right] \\
& + e_x^s \quad z \geqslant L.
\end{aligned} \tag{C2}
$$

Substituting $\sum_{n=0}^{\infty} \gamma^n = \frac{1}{1-\gamma}$ (geometric series sum) and $\gamma = \frac{\sqrt{\varepsilon_{r2}}-1}{\sqrt{\varepsilon_{r2}}+1}$ (reflection coefficient at $z = L$) in the previous

equations and simplifying, we obtain $e_x^d(t \to \infty, z) = e_x^a(t \to \infty, z) = e_x^s$, showing that the electric field distribution into the waveguide at $t \to \infty$ converges to a finite value, equal to the initial electrostatic field value (e_x^s). Following a similar procedure for the magnetic field, it is straightforward to show that $h_y^d(t, z)$ and $h_y^a(t, z)$ in Eqs. (B17) and (B18) converge to zero for $t \to \infty$. Thus, we conclude that after the transient fields induced by the change of the dielectric-block permittivity have passed, the system returns to its initial steady state.

APPENDIX D: CONTINUITY OF ELECTRIC AND MAGNETIC FIELDS AT THE INTERFACE OF A TIME-VARYING DIELECTRIC BLOCK

Here, we examine the continuity of the total tangential components of the electric and magnetic fields across the interface of the time-varying dielectric block after the change of its permittivity ($t > 0$). First, let us evaluate the derived expressions of the electric and magnetic fields in the dielectric and air regions at the location of the interface between the two regions ($z = L$). Plugging $z = L$ in Eqs. (B15) and (B16), we get

$$
e_x^d(t, L) = \frac{e_x^s}{\sqrt{\varepsilon_{r2}} + 1}\left(1 - \frac{\varepsilon_{r1}}{\varepsilon_{r2}}\right)\sum_{n=0}^{\infty} \gamma^n\{u(t - 2nT) + u[t - 2T(1+n)]\} + \frac{\varepsilon_{r1}}{\varepsilon_{r2}}e_x^s u(t), \tag{D1}
$$

$$
e_x^a(t, L) = e_x^s \frac{\sqrt{\varepsilon_{r2}}}{1 - \sqrt{\varepsilon_{r2}}}\left(\frac{\varepsilon_{r1}}{\varepsilon_{r2}} - 1\right)\left[-\gamma u(t) + (1 - \gamma)\sum_{n=1}^{\infty} \gamma^n u(t - 2nT)\right] + e_x^s u(t). \tag{D2}
$$

Subtracting Eq. (D1) from Eq. (D2) and rearranging, we obtain

$$
\begin{aligned}
e_x^d(t, L) - e_x^a(t, L) = {} & \frac{e_x^s}{\sqrt{\varepsilon_{r2}} + 1}\left(1 - \frac{\varepsilon_{r1}}{\varepsilon_{r2}}\right)\left\{(1 + \sqrt{\varepsilon_{r2}})u(t) + [(1 + \gamma) - \sqrt{\varepsilon_{r2}}(1 - \gamma)]\sum_{n=0}^{\infty} \gamma^n u[t - 2(n+1)T]\right\} \\
& + \left(\frac{\varepsilon_{r1}}{\varepsilon_{r2}} - 1\right)e_x^s u(t).
\end{aligned} \tag{D3}
$$

Substituting $\gamma = \frac{\sqrt{\varepsilon_{r2}}-1}{\sqrt{\varepsilon_{r2}}+1}$ in the previous equation, we can readily show that $e_x^d(L, t) - e_x^a(L, t) = 0$ for any $t > 0$. Repeating the same procedure for the magnetic field expressions in Eqs. (B17) and (B18), we get $h_x^d(t, L) - h_x^a(t, L) = 0$ for any $t > 0$. This proves that the electric and magnetic fields across the interface of a time-varying dielectric block immersed in a uniform static electric field are expectedly continuous.

APPENDIX E: INCREASING THE PERMITTIVITY OF THE TIME-VARYING DIELECTRIC BLOCK

In the main text, we have discussed the case when the initial value of the dielectric-block permittivity (ε_{r1}) is suddenly changed in time to a smaller value ($\varepsilon_{r2} < \varepsilon_{r1}$). Here, we discuss the opposite case: The initial value of the dielectric-block permittivity is changed in time to a larger value ($\varepsilon_{r2} > \varepsilon_{r1}$). To this end, we assume that the permittivity of the dielectric block of length L changes abruptly from $\varepsilon_{r1} = 4$ to $\varepsilon_{r2} = 8$ at $t = 0$. This change occurs once a uniform static electric field with intensity $e_x^s = 1\,\text{V/mm}$ has been established inside the waveguide. With this setup, according to the temporal boundary condition, the value of the electrostatic field in the

dielectric region at $t = 0^+$ (right after the permittivity change) is transformed from 1 to 0.5 V/mm, while in the air region it is still equal to 1 V/mm. Analogously to the case discussed in the main text, looking at the electric field distribution inside the waveguide at $t = t_1 = 0.1T$ [see Fig. 6(a)], one can observe a region across the air-dielectric interface where the electric field is continuous and assumes a value between 0.5 and 1 V/mm. From Eqs. (B15) and (B16), we can associate this field with two plane waves ($\frac{1}{2+4\sqrt{2}}u[t_1 - (L - z)/c_d]$ and $-\frac{\sqrt{2}}{1+2\sqrt{2}}u[t_1 - (z - L)/c_a]$) propagating away from the section $z = L$ with velocities equal to the phase velocity of the two media. Figure 6(b) shows the z component of the instantaneous Poynting vector, S_z, at the same time instant
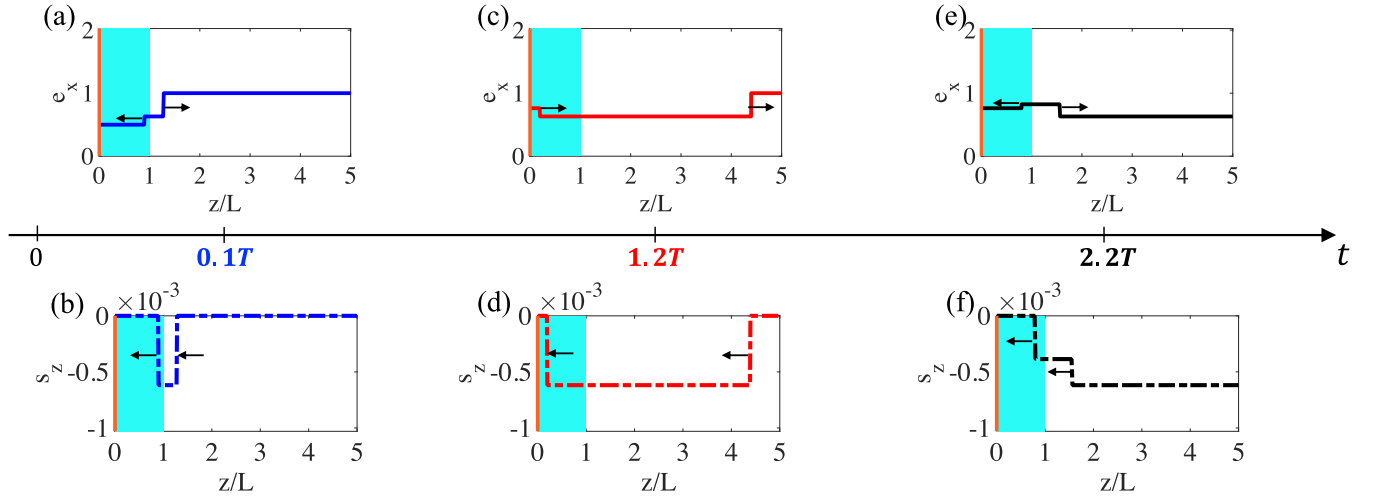
FIG. 6. Spatial distribution of the electric field (a), (c), (e), and the Poynting vector (b), (d), (f), at time instants $t = 0.1T$, $1.2T$, and $2.2T$ when the dielectric block relative permittivity changes from $\varepsilon_{r1} = 4$ to $\varepsilon_{r2} = 8$. The arrows in the top panels (a), (c), (e) and in the bottom panels (b), (d), (f) indicate the direction of propagation of the plane waves and of the corresponding Poynting vectors, respectively.

($t = t_1$). S_z is directed along the negative z axis revealing that the energy flows from the air to the dielectric region, conversely to the case with $\varepsilon_{r2} < \varepsilon_{r1}$. This implies that the right-going plane wave $(-\frac{\sqrt{2}}{1+2\sqrt{2}}u[t_1 - (z-L)/c_a])$, traveling in the air region, is a backward wave while the left-going plane wave $(\frac{1}{2+4\sqrt{2}}u[t_1 - (L-z)/c_d])$, traveling in the dielectric region, is a forward wave. At $t = T$, the left-going plane wave hits the PMC wall generating a second plane wave, $\frac{1}{2+4\sqrt{2}}u[t - (z+L)/c_d]$ [see Eq. (B15)]. This wave, adding to the electric field established by the previous wave, $\frac{1}{2+4\sqrt{2}}u[t - (L-z)/c_d]$, results in the electric field distribution shown in Fig. 6(c) at $t = t_2 = 1.2T$. At this time instant, the air region is still characterized by the same wave $-\frac{\sqrt{2}}{1+2\sqrt{2}}u[t - (z-L)/c_a]$ [see Eq. (B16)] and since $t_2 > t_1$, one can observe it to have traveled further from the air-dielectric interface, as expected. We can notice from Fig. 6(d), displaying S_z at the same time instant ($t = t_2$), that the flow of energy continues having a direction from the air to the dielectric region. At $t = 2T$, the wave traveling in the dielectric region ($\frac{1}{2+4\sqrt{2}}u[t - (z+L)/c_d]$) reaches the spatial discontinuity at $z = L$ and generates a reflected wave, $\frac{2\sqrt{2}-1}{18+8\sqrt{2}}u[t - (L-z)/c_d - 2T]$, and a transmitted wave, $\frac{2\sqrt{2}}{9+4\sqrt{2}}u[t - (z-L)/c_a - 2T]$ [see Eqs. (B15) and (B16),

respectively]. These reflected and transmitted waves are added to the electric field established by the previous waves in the dielectric and air regions, respectively, resulting in the distribution at $t = t_3 = 2.2T$ shown in Fig. 6(e). The energy continues flowing from the air to the dielectric region as shown in Fig. 6(f). As time passes, the multiple reflection process, due to the spatial boundary at $z = 0$ and $z = L$, continues increasing the number of plane waves propagating into the waveguiding system as described by Eqs. (B15) and (B16). In contrast to the case with $\varepsilon_{r2} < \varepsilon_{r1}$ discussed in the main text, increasing the permittivity of the dielectric block ($\varepsilon_{r2} > \varepsilon_{r1}$) results in waves in both regions carrying energy from the air to the dielectric region. The air region is temporarily depleted from its energy by waves traveling away from the air region toward the dielectric region. This energy is transferred to the dielectric region and is restored to its original value at $t \to \infty$.

APPENDIX F: TOTAL RADIATED ENERGY DENSITY

In this Appendix, we derive and discuss the total radiated energy density carried by the infinite set of plane waves traveling in the air region. First, we evaluate the instantaneous Poynting vector, $S_z^a(z, t) = e_x^a(z, t)h_y^a(z, t)$, which results in

$$
S_z^a(z, t) = \frac{(e_x^s)^2}{\mu_0 c_a} \frac{\varepsilon_{r2}}{(1 - \sqrt{\varepsilon_{r2}})^2} \left(\frac{\varepsilon_{r1}}{\varepsilon_{r2}} - 1\right)^2 \sum_{n=1}^{\infty} \gamma^{2n} \left\{ u\left[t - \frac{z - L}{c_a} - 2(n-1)T\right] - u\left(t - \frac{z - L}{c_a} - 2nT\right) \right\}
$$
$$
+ \frac{(e_x^s)^2}{\mu_0 c_a} \frac{\sqrt{\varepsilon_{r2}}}{1 - \sqrt{\varepsilon_{r2}}} \left(1 - \frac{\varepsilon_{r1}}{\varepsilon_{r2}}\right) \sum_{n=1}^{\infty} \gamma^n \left\{ u\left[t - \frac{z - L}{c_a} - 2(n-1)T\right] - u\left(t - \frac{z - L}{c_a} - 2nT\right) \right\}. \quad \text{(F1)}
$$

Integrating the previous equation from $t = 0$ to $t \to \infty$, we obtain the total radiated energy per unit area,

$$
W_{\text{rad}} = \frac{1}{2} \frac{\varepsilon_0}{\varepsilon_{r2}} L (\varepsilon_{r1}^2 - \varepsilon_{r2}^2) \left(\frac{V}{d}\right)^2. \quad \text{(F2)}
$$

One can notice that $W_{\text{rad}} + \Delta W_\infty = 0$, with ΔW_∞ denoting, as indicated in the main text, the difference of the electrostatic energy per unit area stored in the dielectric block at $t = 0^+$ and $t \to \infty$. The latter equation highlights that
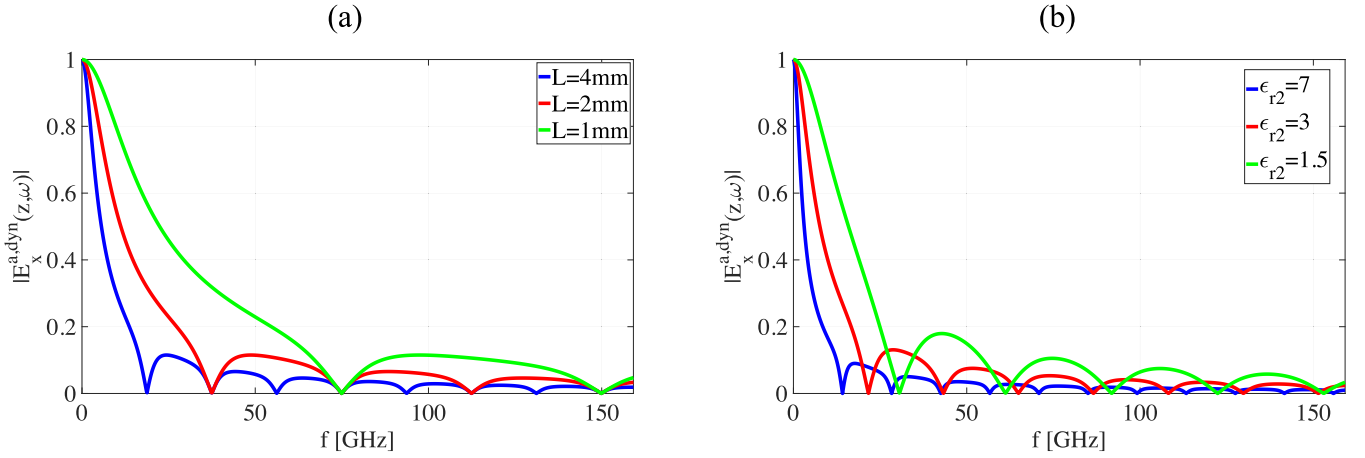
(a)　　　　　　　　　　　　　　　　　　　　　(b)

FIG. 7. Magnitude of the frequency spectrum of the dynamic electric field in the air region normalized to maximum (a) for different values of L ($\varepsilon_{r1} = 8$ and $\varepsilon_{r1} = 4$) and (b) ε_{r2} ($\varepsilon_{r1} = 8$ and $L = 4\,\text{mm}$).

the growth (reduction) of the electrostatic energy in the dielectric block induced by the change of its permittivity is fully released (restored) through the electromagnetic energy propagating in the air region.

APPENDIX G: FOURIER SPECTRUM OF THE ELECTRIC FIELD IN THE AIR REGION

The frequency spectrum of the electric field in the air region can be easily obtained by applying a Fourier transform to $e_x^a(z, t)$ [Eq. (B20)], $E_x^a(z, \omega) = \int_0^\infty e_x^a(z, t) e^{-i\omega t} dt$, which gives

$$E_x^a(z, \omega) = \frac{2e_x^s \sqrt{\varepsilon_{r2}}}{1 + \sqrt{\varepsilon_{r2}}} \left(\frac{\varepsilon_{r1}}{\varepsilon_{r2}} - 1 \right) \frac{\sin(\omega T)}{\omega} \frac{e^{-i\omega\left(\frac{z-L}{c_a} + T\right)}}{1 - \gamma e^{-i2\omega T}} + \frac{e_x^s}{i\omega},$$

(G1)

with $\omega = 2\pi f$ and f is the frequency. $E_x^a(z, \omega)$, analogously to its time-domain counterpart, is given by the superposition of two terms. The first one, $E_x^{a,dyn}(z, \omega) = \frac{2e_x^s \sqrt{\varepsilon_{r2}}}{1 + \sqrt{\varepsilon_{r2}}} \left(\frac{\varepsilon_{r1}}{\varepsilon_{r2}} - 1 \right) \frac{\sin(\omega T)}{\omega} \frac{e^{-i\omega\left(\frac{z-L}{c_a} + T\right)}}{1 - \gamma e^{-i2\omega T}}$, represents the spectrum of the dynamic field, while the second one, $E_x^{a,dc}(z, \omega) = \frac{e_x^s}{i\omega}$, represents the spectrum of the static field. It is evident from the expression of $E_x^{a,dyn}(z, \omega)$ that its magnitude follows the shape of a sinc function and goes to zero whenever $\omega = p\pi/T$ [$f = p/(2T)$] with $p = 1, 2, 3, \ldots$. Thus, the frequency spectrum of the dynamic electric field in the air region is maximum at $f = 0$ and has nulls at equally spaced frequency intervals of $1/(2T)$. Since $T = L/c_d$, the nulls move toward higher frequencies for a smaller L or ε_{r2}, as shown in Fig. 7. In other words, the spectrum of the field becomes broader as L or ε_{r2} decrease.

APPENDIX H: SMOOTH TEMPORAL VARIATION OF THE DIELECTRIC-BLOCK PERMITTIVITY

In this Appendix, we extend our investigation of static-to-dynamic field conversion with suddenly changing dielectric permittivity to the case of smoothly varying dielectric permittivity in time. To this end, we assume that the relative

permittivity of the dielectric block in Fig. 2(b) varies from $\varepsilon_{r1} = 8$ to $\varepsilon_{r2} = 4$ during a temporal interval $\tau > 0$, as shown in the inset of Fig. 8. With this setup, the numerical results of the electric field inside the air region ($z = 20\,\text{mm}$) for four different values of τ are shown in Fig. 8. One can observe that for τ much smaller than the propagation time between the air-dielectric interface and the magnetic wall ($T = 20$ [ps] for the case under consideration) the numerical solutions agree pretty well with the analytical one (continuous black line) derived in this manuscript assuming an abrupt change of the dielectric-block permittivity. By increasing τ, the edges of the rectangular pulses become less sharp, up to the point that the temporal distribution of the electric field is a single pulse. As expected, the analytical solution derived in this manuscript for the sudden change of permittivity approximately applies to smooth temporal variation of the permittivity, as long as the transition time (τ) is much smaller than T. However, the
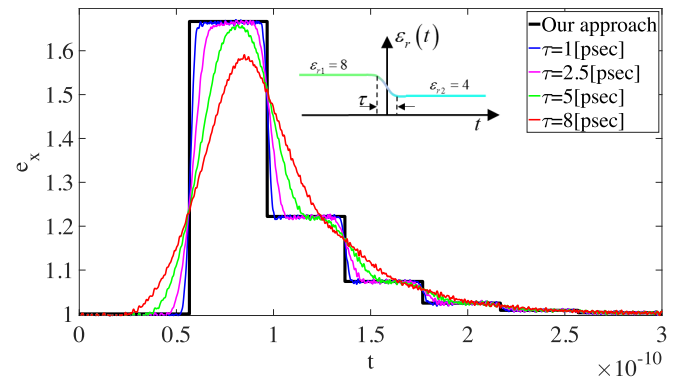

FIG. 8. Numerically evaluated electric field as a function of time at the location $z = 20\,\text{mm}$ inside the air region of the waveguiding system of Fig. 2(b) assuming the relative permittivity of the dielectric block changes from $\varepsilon_{r1} = 8$ to $\varepsilon_{r1} = 4$ with four different transition times τ (blue, magenta, green, and red curves). The inset shows the temporal function of the relative permittivity $\varepsilon_r(t)$. The black curve, representing the temporal evolution of the electric field at the same location ($z = 20\,\text{mm}$), is obtained from Eq. (B16). The dielectric block length (L) is assumed to be 3 mm.

results shown in Fig. 8 reveal that the effect of static-to-dynamic field conversion with time-varying media preserves even for gradual variation of the permittivity.

APPENDIX I: POTENTIAL PATHWAY FOR FUTURE EXPERIMENTAL VERIFICATIONS

Here, we briefly discuss the possibilities for future experimental demonstrating of our theoretical proposal investigated in this paper. Building upon the current state of the art experiments related to the time-dependent media, we can suggest three possible pathways to demonstrate such conversion of electrostatic fields to dynamic fields with time-varying media. The first two are at low frequencies in a transmission line scenario. The third one is at near-infrared (NIR) frequencies based on materials operating at the epsilon near zero (ENZ) regime. The first pathway is based on a variable capacitor whose capacitance is controlled mechanically such as Micro-electromechanical systems (MEMS) capacitors [19]. By using these capacitors, one can envision the possibility to experimentally test the phenomenon described in this work in the following manner. One can connect such a capacitor to a DC voltage source through a transmission line. Once the DC source has fully charged the capacitor, we change its capacitance in time. The voltage pulse induced from the capacitance temporal variation and traveling toward the DC source can be measured by connecting an oscilloscope along the transmission line. The switching time of standard MEMS capacitors is on the order of $10\,[\mu s]$ [19].

As for the second pathway, a setup similar to the previous one can be explored. However, instead of using a mechanically controlled capacitor, the transmission line can be terminated with a set of shunt capacitors, which, charged with the DC voltage source, mimic a dielectric slab with effective permittivity. The shunt capacitors can then be connected to another set of parallel capacitors using electronic switches. By turning the switches on and off, one can modulate the capacitance of the shunt capacitors in time, resulting in a temporal modulation of their effective permittivity. With this approach, one can achieve faster temporal variation of the effective permittivity (smaller than 0.1 [ns] [20]), so it will be less challenging to experimentally realize the effect of stepwise permittivity modulation.

The third pathway to demonstrate our proposal in a laboratory relies on ENZ material [21,22]. It was recently shown that the family of transparent conductive oxides (TCO) operating close to the ENZ point (real part of the permittivity near zero) represents a promising platform to experimentally demonstrate new wave phenomena in the optical (or near-infrared) regime enabled by time-varying media [23]. Specifically, this study has reported that, upon illuminating with an ultrashort pulse, an Al-doped ZnO (AZO) film with an ENZ region occurring around the wavelength $\lambda = 1500\,\text{nm}$ can exhibit a large (order of unity) and fast (order of femtoseconds) variation of its refractive index. Building on this work, one may envision the possibility to test the phenomenon of static-to-dynamic field conversion with time-varying media investigated in this paper in the IR regime.

---

[1] F. R. Morgenthaler, Velocity modulation of electromagnetic waves, IEEE Trans. Microwave Theory Tech. **6**, 167 (1958).

[2] L. B. Felsen and G. M. Whitman, Wave propagation in time-varying media, IEEE Trans. Antennas Propag. **18**, 242 (1970).

[3] R. Fante, Transmission of electromagnetic waves into time-varying media, IEEE Trans. Antennas Propag. **19**, 417 (1971).

[4] A. A. Oliner and A. Hessel, Wave propagation in a medium with a progressive sinusoidal disturbance, IEEE Trans. Microwave Theory Tech. **9**, 337 (1961).

[5] N. A. Estep, D. L. Sounas, J. Soric, and A. Alù, Magnetic-free non-reciprocity and isolation based on parametrically modulated coupled-resonator loops, Nat. Phys. **10**, 923 (2014).

[6] D. G. Baranov, A. Krasnok, and A. Alù, Coherent virtual absorption based on complex zero excitation for ideal light capturing, Optica **4**, 1457 (2017).

[7] D. L. Sounas, Virtual perfect absorption through modulation of the radiative decay rate, Phys. Rev. B **101**, 104303 (2020).

[8] V. Pacheco-Peña and N. Engheta, Temporal aiming, Light Sci. Appl. **9**, 129 (2020).

[9] V. L. Ginzburg, Transition radiation and transition scattering, Phys. Scr. **1982**, 182 (1982).

[10] W. B. Mori, T. Katsouleas, J. M. Dawson, and C. H. Lai, Conversion of dc Fields in a Capacitor Array to Radiation by a Relativistic Ionization Front, Phys. Rev. Lett. **74**, 542 (1995).

[11] C. H. Lai, R. Liou, T. C. Katsouleas, P. Muggli, R. Brogle, C. Joshi, and W. B. Mori, Demonstration of Microwave Genera-

tion from a Static Field by a Relativistic Ionization Front in a Capacitor Array, Phys. Rev. Lett. **77**, 4764 (1996).

[12] E. Esarey, P. Sprangle, B. Hafizi, and P. Serafim, Radiation generation by photoswitched, periodically biased semiconductors, Phys. Rev. E **53**, 6419 (1996).

[13] S. C. Wilks, J. M. Dawson, W. B. Mori, T. Katsouleas, and M. E. Jones, Photon Accelerator, Phys. Rev. Lett. **62**, 2600 (1989).

[14] C. D. Murphy, R. Trines, J. Vieira, A. J. W. Reitsma, R. Bingham, J. L. Collier, E. J. Divall, P. S. Foster, C. J. Hooker, A. J. Langley, P. A. Norreys, R. A. Fonseca, F. Fiuza, L. O. Silva, J. T. Mendonça, W. B. Mori, J. G. Gallacher, R. Viskup, D. A. Jaroszynski, S. P. D. Mangles *et al.*, Evidence of photon acceleration by laser wake fields, Phys. Plasmas **13**, 033108 (2006).

[15] D. M. Solís, R. Kastner, and N. Engheta, Time-varying materials in presence of dispersion: Plane-wave propagation in a Lorentzian medium with temporal discontinuity, Photonics Res. **9**, 1842 (2021).

[16] Y. Xiao, D. N. Maywar, and G. P. Agrawal, Reflection and transmission of electromagnetic waves at a temporal boundary, Opt. Lett. **39**, 574 (2014).

[17] J. A. Stratton, *Electromagnetic Theory* (McGraw-Hill, New York, 1940).

[18] M. R. Spiegel, *Laplace Transforms* (McGraw-Hill Education, New York, 1986).

[19] J. Zou, C. Liu, J. Schutt-Aine, J. Chen, and S.-M. Kang, Development of a wide tuning range MEMS tunable capacitor for wireless communication systems, in *International Electron Devices Meeting 2000, Technical Digest IEDM* (IEEE, New York, 2000).

[20] T. Dinc, M. Tymchenko, A. Nagulu, D. Sounas, A. Alu, and H. Krishnaswamy, Synchronized conductivity modulation to realize broadband lossless magnetic-free non-reciprocity, Nat. Commun. **8**, 795 (2017).

[21] N. Engheta, Pursuing near-zero response, Science **340**, 286 (2013).

[22] I. Liberal and N. Engheta, The rise of near-zero-index technologies, Science **358**, 1540 (2017).

[23] E. Lustig, S. Saha, E. Bordo, C. DeVault, S. N. Chowdhury, Y. Sharabi, A. Boltasseva, O. Cohen, V. M. Shalaev, and M. Segev, Towards photonic time-crystals: Observation of a femtosecond time-boundary in the refractive index, in *Conference on Lasers and Electro-Optics, OSA Technical Digest* (OSA, Washington, DC, 2021).